JOURNAL OF MATERIALS SCIENCE 33 (1998) 2563–2571

Stress-induced phase transformations in a hot-deformed two-phase ($\alpha_2 + \gamma$) TiAl alloy

J. G. WANG*‡§, L. C. ZHANG*, G. L. CHEN*, H. Q. YE‡
*State Key Laboratory for Advanced Metals and Materials, University of Science and Technology Beijing, Beijing 100083, People's Republic of China
‡Laboratory of Atomic Imaging of Solids, Institute of Metal Research, Academia Sinica, Shenyang 110015, People's Republic of China

Stress-induced $\gamma \rightarrow \alpha_2$, $\alpha_2 \rightarrow \gamma$ and $\gamma \rightarrow$ 9R phase transformations in a hot-deformed Ti–45 at % Al–10 at % Nb alloy have been investigated using high-resolution transmission electron microscopy. The $\gamma \rightarrow \alpha_2$ phase transformation is an interface-related process. The interfacial superdislocations emitted from the misoriented semicoherent α_2–γ interface react with each other or with the moving dislocations in the γ phase, resulting in the formation of the α_2 phase. The nucleation of the $\alpha_2 \rightarrow \gamma$ phase transformation takes place either at the α_2–γ interfaces or at the stacking faults on the basal plane of α_2 phase, and the growth of γ plate is accomplished by the moving of $a/6\langle 1\,0\,\bar{1}\,0\rangle$ Shockley partials on alternate basal plane $(0\,0\,0\,1)_{\alpha_2}$. The 9R structure was usually found to form at incoherent twin or pseudotwin boundaries. During deformation the interfacial Shockley partial dislocations of these incoherent twin and pseudotwin boundaries may glide on $(1\,1\,1)_\gamma$ planes into the matrix, resulting in the formation of 9R structure. The interfaces (including α_2–γ and γ–γ interfaces) as well as the crystallographic orientation relationship between the as-received or stress-induced α_2, γ and 9R phase have been analysed. The mechanisms for the stress-induced $\gamma \rightarrow \alpha_2$, $\alpha_2 \rightarrow \gamma$ and $\gamma \rightarrow$ 9R phase transformations were also discussed.

1. Introduction

It is widely accepted that two-phase γ-TiAl alloys as viable structural materials depends strongly on the optimization of the designed microstructures which can be produced by controlled processing and appropriate alloying [1]. Recently, development of microstructures by thermomechanical treatment is under intensive investigation so as to develop balanced improvements of properties [1]. During thermomechanical processing, the lamellar structure is heavily deformed and simultaneously recrystallized; a variety of high-temperature deformation modes such as ordered twinning of the $\{1\,1\,1\}\langle 1\,1\,\bar{2}]$ type, slip on $\{1\,1\,1\}\langle\bar{1}\,1\,0]$ and $\langle\bar{1}\,0\,1]$, $\frac{1}{2}\langle 1\,1\,\bar{2}]$ superdislocation slips occur at the same time [2–4]. Accompanying these deformation modes, there also exist some stress-induced phase transformations including $\gamma \rightarrow$ 9R, $\gamma \rightarrow \alpha_2$ and $\alpha_2 \rightarrow \gamma$ [5].

In fact, the stress-induced structural transition phenomena have been reported by some researchers in some intermetallics under high-temperature or room-temperature deformation. Stress-induced disordering characterized as the modification of the superdislocation from fourfold to twofold and to single dislocation, and creep-induced reordering characterized as the modification of the superdislocation from twofold to fourfold, may occur in Fe_3Al alloy. During creep, two opposite phenomena, i.e., strain-induced disordering and creep-induced reordering, are in competition [6]. More recently, many researchers reported that stress-induced phase transformations occur during deformation of two-phase γ-TiAl alloys. For example, Singh and Howe [7] observed the formation of the stress-induced 9R structure in a Ti–48.7 at % Al alloy deformed to 12% compressive strain at room temperature, Appel *et al.* [8] also observed the formation of 9R structure in a Ti–48.5 at % Al–1.5 at % Mn alloy deformed in tension at 900 °C, Feng *et al.* [9,10] reported the formation of Ti_3Al phase within the primary TiAl (i.e., a stress-induced $\gamma \rightarrow \alpha_2$ phase transformation) during deformation of XD^{TM} (Ti–45 at % Al)–TiB_2 alloys, Gao *et al.* [11] verified the existence of such a stress-induced $\gamma \rightarrow \alpha_2$ phase transformation in a Ti–47.5 at % Al–2.5 at % V alloy compressed at room temperature and claimed that the stress–strain curve of such a stress-induced $\gamma \rightarrow \alpha_2$ phase transformation appears to be similar to that of stress-induced $\beta_1 \rightarrow \gamma_1$ martensitic transformations in Cu–Al–Ni alloys and Zhang *et al.* [12] reported a stress-induced $\alpha_2 \rightarrow \gamma$ phase transformation in a Ti–50

§*Present address*: Lawrence Livermore National Laboratory, PO Box 808, L-370, Livermore, CA 94551-9900, USA. E-mail: wang21@llnl.gov.

at % Al–2 at % Mn–1 at % Nb alloy compressed to 1–2% at room temperature. However, the mechanisms of these stress-induced phase transformations in two-phase γ-TiAl alloys have not been studied in detail.

Ti–45 at % Al–10 at % Nb is a high-performance alloy with excellent high-temperature strength and oxidation resistance [13]. As a part of our systematic continual research on the stress-induced microstructures and phase transitions in Ti–Al–Nb ternary intermetallic alloys [13–18], in this paper, stress-induced $\gamma \rightarrow \alpha_2$, $\alpha_2 \rightarrow \gamma$ and $\gamma \rightarrow 9R$ phase transformations in a hot-worked Ti–45 at % Al–10 at % Nb alloy with nearly fully lamellar microstructure were investigated by high-resolution transmission electron microscopy (HRTEM). The mechanisms for the stress-induced $\gamma \rightarrow \alpha_2$, $\alpha_2 \rightarrow \gamma$ and $\gamma \rightarrow 9R$ phase transformations were also discussed.

2. Experimental procedure

The alloy with a composition 45 at % Ti, 45 at % Al and 10 at % Nb was prepared from high-purity Ti (99.9%), Al (99.9%) and Nb (99.9%) by non-consumable electrode arc melting in a purified argon atmosphere. The as-cast ingot was wrapped in a steel foil, heated to 1250 °C for 30 min and then quasi-isothermally forged to more than 40%. The temperature of the forge hammer was 1050 °C and the strain rate was about $5 \times 10^{-1}\ s^{-1}$. The forged ingot was air cooled.

Transmission electron microscopy (TEM) specimens were prepared by standard twin-jet polishing and/or ion milling and examined using a JEOL-2000EXII electron microscope operating at 200 kV with a spherical aberration coefficient of 0.7 mm.

3. Results

The phase constitution and the microstructure of the alloy were studied previously [13, 14]. The phases in the alloy were γ-TiAl and α_2-Ti_3Al as analysed by X-ray diffraction. The microstructure of the quasi-isothermal forged Ti–45 at % Al–10 at % Nb alloy observed by conventional TEM was a nearly lamellar microstructure with a high volume fraction (>95%) of lamellar colonies. During hot working, the lamellar structure is deformed and simultaneously dynamically recovered or partially recrystallized. The dynamic recrystallization of the deformed lamellar structure was found to maintain the lamellar morphology in the lamellar colonies.

3.1. Stress-induced $\gamma \rightarrow \alpha_2$ phase transformation

Fig. 1 shows a HRTEM image of an α_2–γ_C lamellar structure in $[1\,0\,\bar{1}]_\gamma // [1\,1\,\bar{2}\,0]_{\alpha_2}$ orientation (here the symbols γ_A, γ_B, γ_C, γ_D, γ_E and γ_F are used to distinguish six γ variants with $[\bar{1}\,1\,0]$, $[1\,\bar{1}\,0]$, $[1\,0\,\bar{1}]$, $[\bar{1}\,0\,1]$, $[0\,\bar{1}\,1]$ and $[0\,1\,\bar{1}]$ orientations, respectively [19, 20]). The interface between the α_2 and γ_C phases is a misoriented semicoherent interphase boundary with the

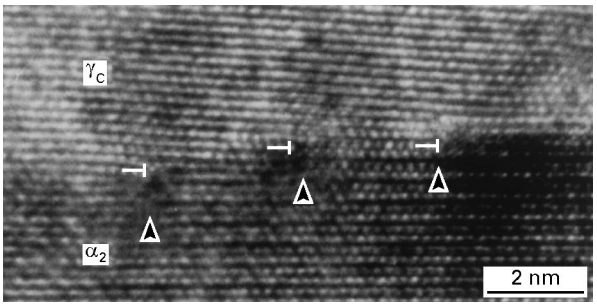

Figure 1 HRTEM image of a deviating semicoherent α_2–γ interface with deviation angle $\theta = 2.5°$, i.e., the orientation relationship between the γ and the α_2 phase is $[1\,0\,\bar{1}]_\gamma // [1\,1\,\bar{2}\,0]_{\gamma_2}$ and $(1\,1\,1)_\gamma \wedge (0\,0\,0\,1)_{\alpha_2} \approx 2.5°$.

$(1\,1\,1)_\gamma$ plane misoriented by $\theta = 2.5°$ from the $(0\,0\,0\,1)_{\alpha_2}$, i.e., the orientation relationship between the γ and α_2 phase is $[1\,0\,\bar{1}]_\gamma // [1\,1\,\bar{2}\,0]_{\alpha_2}$ and $(1\,1\,1)_\gamma \wedge (0\,0\,0\,1)_{\alpha_2} \approx 2.5°$. Ledges that were three $(1\,1\,1)_\gamma$ or $(0\,0\,0\,1)_{\alpha_2}$ atomic planes high were observed and some ledges are indicated by arrows in Fig. 1. The deviation arises from the climb component of the ledge dislocation: $\frac{1}{3}[1\,1\,1]$ Frank partials. This can be considered to arise because the $\alpha_2 - \gamma$ interface can absorb the slipping dislocations in the γ phase as a dislocation sink to adjust the deformation. The characteristics of ledge dislocations at the interface have been determined as $\frac{1}{2}[1\,0\,1] \rightarrow \frac{1}{6}[1\,\bar{2}\,1] + \frac{1}{3}[1\,1\,1]$, i.e., 90° Shockley partial dislocation + $\frac{1}{3}[1\,1\,1]$ Frank partial dislocation [14, 15]. It can be seen from Fig. 1 that the dislocation ledges contain $\frac{1}{3}[1\,1\,1]$ Frank partial dislocations (see arrows in Fig. 1). The mean distances of these ledges are about 4.6 nm. A dark contrast near the ledges reveals that there exist high stresses which are associated with the Frank-type dislocations.

Fig. 2a shows a lamellar structure composed of γ_C–γ_D–α_2, where the γ_D–α_2 interface is also a misoriented semicoherent α_2–γ interface with the deviation angle $\theta = 2.5°$. Above this interface, a thin stress-induced α_2 plate (here referred to as DI-α_2) about 25 nm long and 2.5 nm thick forms in the γ_D lamellae; meanwhile the γ phase between the α_2 lamella and the DI-α_2 plate changes from γ_D to γ_B. Fig. 2b is the enlarged view of the region containing DI-α_2. Both the orientation relationships between γ_B and as-received α_2 and the orientation relationships between γ_B and DI-α_2 are nearly exactly $[1\,\bar{1}\,0]_\gamma // [1\,1\,\bar{2}\,0]_{\alpha_2}$ and $(1\,1\,1)_\gamma // (0\,0\,0\,1)_{\alpha_2}$. However, the orientation relationship between DI-α_2 and as-accepted γ_D is not exactly $[\bar{1}\,0\,1]_\gamma // [1\,1\,\bar{2}\,0]_{\alpha_2}$ and $(1\,1\,1)_\gamma // (0\,0\,0\,1)_{\alpha_2}$; a deviation angle $\theta \approx 2.5°$ existed between the $(1\,1\,1)_{\gamma_D}$ and the $(0\,0\,0\,1)_{DI-\alpha_2}$ plane. Also, there is a similar deviation angle between $(1\,1\,1)_{\gamma_B}$ and $(1\,1\,1)_{\gamma_D}$ planes. $\frac{1}{3}[1\,1\,1]$ Frank partial dislocations are observed at both the γ_D–DI-α_2 interface and the γ_D–γ_B boundary.

Fig. 3a shows a well-grown DI-α_2 plate near the misoriented semicoherent α_2–γ_D interface. It is about 5 nm thick and as long as the whole image. Also, the γ phase between the α_2 lamellae and the DI-α_2 plate changes from γ_D to γ_B, and it is divided into many blocks by stacking faults on $(1\,\bar{1}\,1)$ plane which are

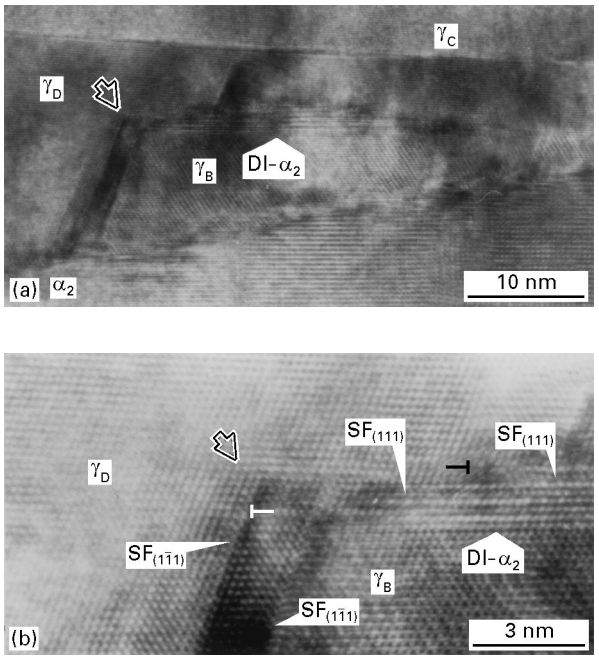

Figure 2 (a) HRTEM image showing a thin deformation-induced α_2 plate (here referred to as DI-α_2) formed in the γ lamellae near a deviating semicoherent α_2–γ interface with deviation angle $\theta = 2.5^\circ$; (b) the enlarged view of the region containing DI-α_2.

either associated with a ledge at the γ_B–DI-α_2 interface or suspended in the γ_B phase. The enlargement of regions A, B and C in Fig. 3a are shown in Fig. 3b, c and d, respectively, where region A is the area containing the "tip" of the stress-induced α_2 plate and region C is the area containing many stacking faults terminated at the middle of the γ_B phase. (In fact, beyond the stacking faults the γ phase between the DI-α_2 and the α_2 phases still remains as γ_D). From Fig. 3b, it can be seen that there exist many ledges at the DI-α_2–γ_B interface, and each ledge is associated with a stacking fault on $(1\,\bar{1}\,1)$ plane; also $\frac{1}{3}[1\,1\,1]$ Frank partial dislocations can be observed either on the DI-α_2–γ_D interface or at the ledge of the DI-α_2–γ_B interface. The "tip" of the DI-α_2 plate, which is indicated by a black arrowhead in Fig. 3b, is actually a stacking fault on the $(1\,1\,1)$ plane. A stacking fault on the $(1\,1\,1)$ plane accompanying a climb of a $\frac{1}{3}[1\,1\,1]$ Frank partial dislocation, which is emitted from the misoriented semicoherent α_2–γ interfaces, intersects the stacking fault on the $(1\,\bar{1}\,1)$ plane. In Fig. 3d, many stacking faults on $(1\,\bar{1}\,1)$ planes stemming from the ledges on the misoriented semicoherent α_2–γ interface terminate in the middle part of the γ phase. Accompanying the propagation of these stacking faults into the γ phase on the $(1\,\bar{1}\,1)$ planes, $\frac{1}{3}$ $[1\,1\,1]$ Frank partial dislocations are also observed to climb along the $(1\,\bar{1}\,1)$ plane from the misoriented semicoherent $\alpha_2 - \gamma$ interface into the γ phase. This means that the stress-induced $\gamma \rightarrow \alpha_2$ phase transformation is an interphase interface-related process. The structure of the dislocation ledges on the misoriented semicoherent α_2–γ interface is expected to play an important role in the formation of the stress-induced α_2 phase plate, and this will be discussed below.

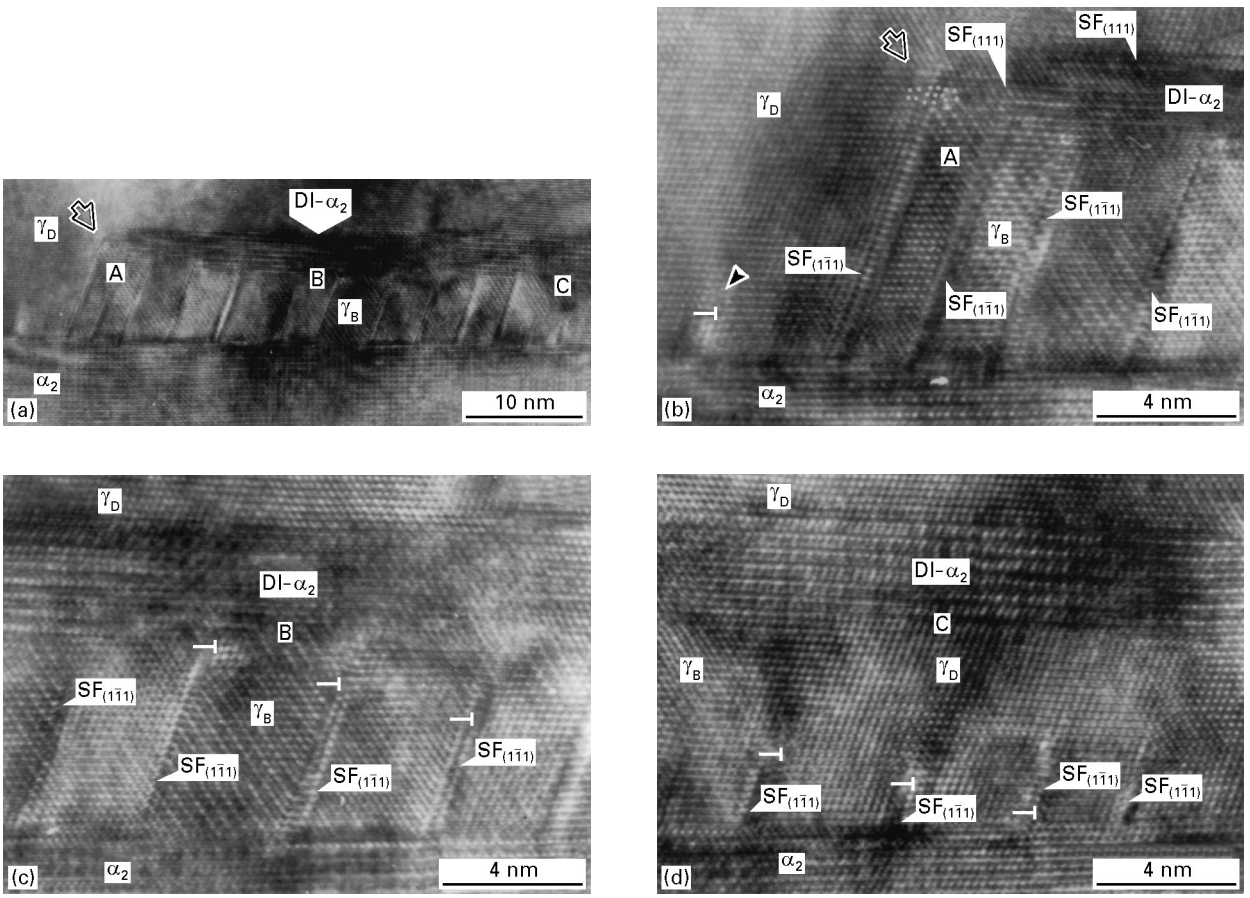

Figure 3 (a) HRTEM image showing a well-grown DI-α_2 plate near the deviating semicoherent α_2–γ_D interface; (b), (c) and (d) enlargements of the regions A, B and C, respectively, in (a).

3.2. Stress-induced $\alpha_2 \rightarrow \gamma$ phase transformation

In Fig. 4a the α_2 lamellae is separated into two parts by a stress-induced γ(DI-γ) plate. This DI-γ phase plate is nucleated during deformation at the misoriented semicoherent α_2–γ_D interface and penetrates into the α_2 phase. The orientation relationship between the α_2 and the DI-γ plate is exactly $[1\,1\,\bar{2}\,0]_{\alpha_2}//[1\,0\,\bar{1}]_{DI-\gamma}$ and $(0\,0\,0\,1)_{\alpha_2}//(1\,1\,1)_{DI\text{-}\gamma}$. The (1 1 1) plane of γ_D and the (1 1 1) plane of DI-γ enclose an angle of about 2.5°. Fig. 4b shows the tip of the DI-γ plate. Rather high stresses exist in this area so that it is very difficult to obtain a well-resolved HRTEM image. At the tip of the DI-γ plate, stacking-fault fringes can be seen in the α_2 matrix (see arrowheads). Also, it can be seen that these stacking fault fringes penetrate into the α_2 matrix in coordination. This means that the $\alpha_2 \rightarrow$ DI-γ transformation is accomplished by the glide of $(a/6\langle 1\,0\,\bar{1}\,0\rangle$ Shockley partials on the alternate basal plane $(0\,0\,0\,1)_{\alpha_2}$, and the $(a/6)\langle 1\,0\,\bar{1}\,0\rangle$ Shockley partials move in coordination rather than to sweep on the $(0\,0\,0\,1)_{\alpha_2}$ plane one by one.

Fig. 5a shows a HRTEM image of a deformed α_2 lamellae in the $\langle 1\,1\,\bar{2}\,0\rangle_{\alpha_2}$ orientation. Three stacking faults A, B and C on the $(0\,0\,0\,1)_{\alpha_2}$ plane are observed. Stacking fault C is a simple stacking fault, while at the middle part of stacking faults A and B there exist three or four layers of the basal planes in the ABC... stacking sequence, respectively (see Fig. 5b and c). In fact such an ABCABC... stacking sequence would result in a structure change from α_2 to face-centred cubic (f.c.c.). Also, in Fig. 5a, a well-grown DI-γ (as indicated at D) can be seen; the "head" of this DI-γ plate is observed to be stacking faults of α_2 phase (see arrowheads).

3.3. Stress-induced $\gamma \rightarrow$ 9R structures

3.3.1. Observation of the 9R structure

Three kinds of interface can be formed between two lamellae of either variant: true twin boundary (γ_A–γ_B

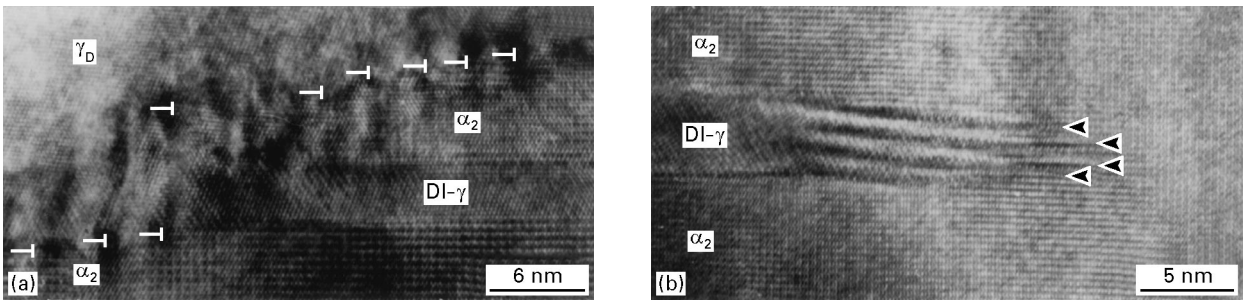

Figure 4 (a) HRTEM image showing a DI-γ phase plate formed at the deviating semicoherent α_2–γ_D interface penetrating into the α_2 phase; (b) HRTEM image showing the tip of the DI-γ plate.

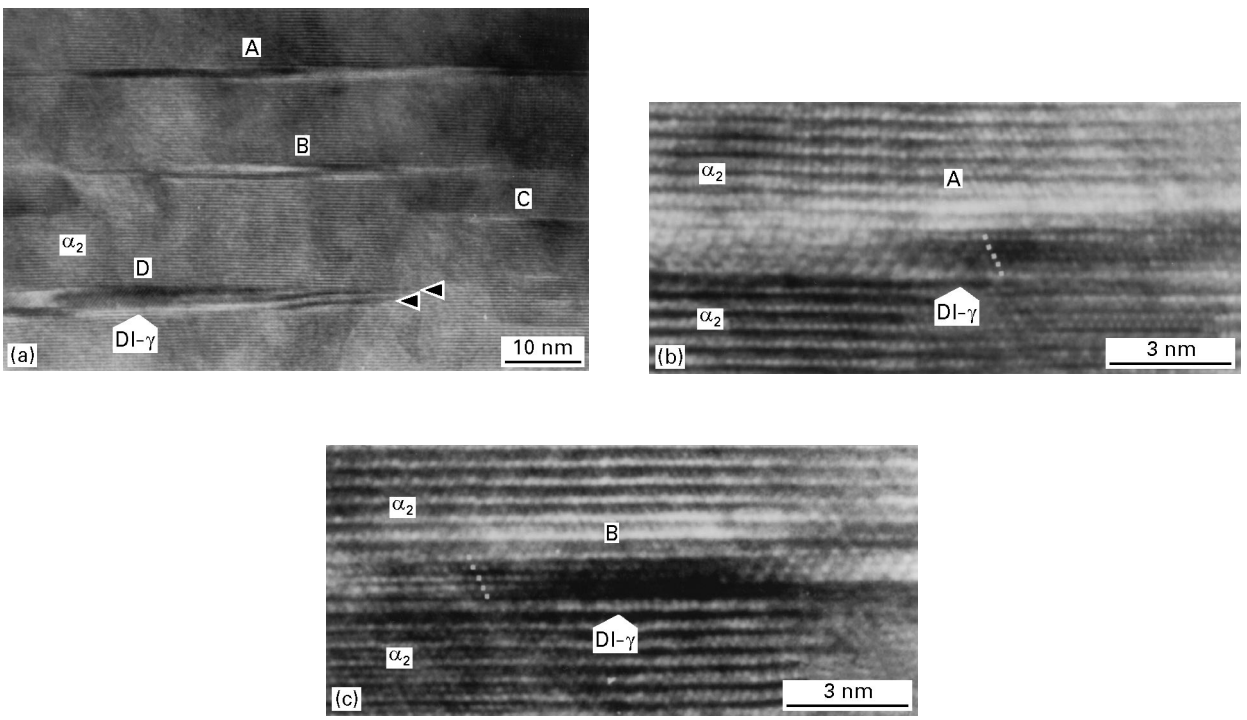

Figure 5 (a) HRTEM image of a deformed α_2 lamellae in the $\langle 1\,1\,2\,0\rangle_{\alpha_2}$ orientation showing DI-γ laths formed at stacking faults on the $(0\,0\,0\,1)_{\alpha_2}$ planes of the α_2 phase; (b) and (c) enlargements of stacking faults A and B, respectively in (a) showing four and three layers of the basal planes in the ABC… stacking sequence.

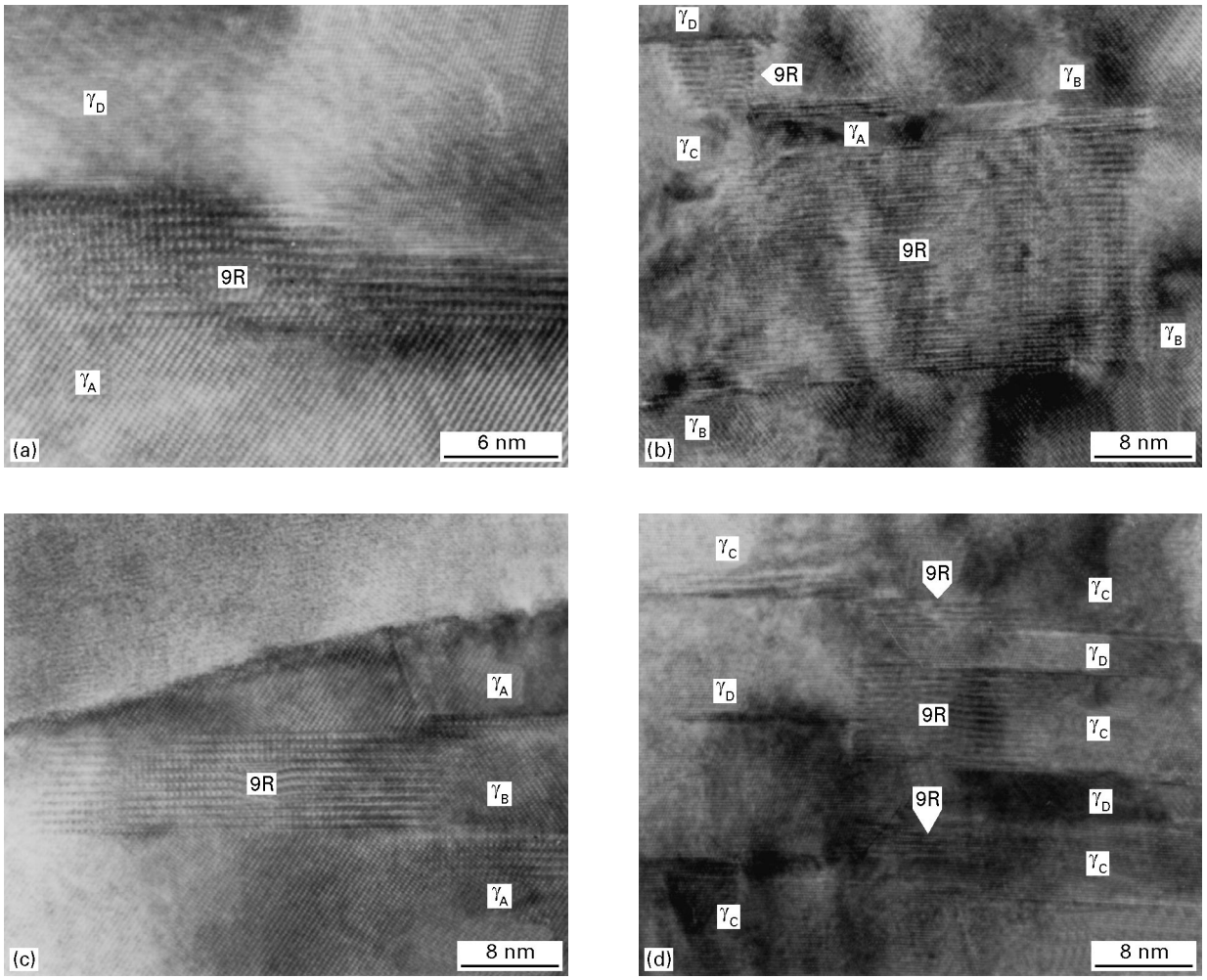

Figure 6 HRTEM images of the 9R structure formed (a), (b) at multiple-height ledges of pseudotwin boundaries and (c), (d) at multiple-height ledges of twin boundaries.

or γ_C–γ_D), pseudotwin boundary (γ_A–γ_D or γ_B–γ_C) and 120°-rotation-type boundary (γ_A–γ_C or γ_B–γ_D) [14, 15, 19, 20]. Fig. 6 shows HRTEM images of various γ variants and stress-induced structures with a three-plane periodicity (hereafter referred to as 9R) in the quasi-isothermally forged sample. Fig. 6a shows a pseudotwin γ_D–γ_A boundary; the 9R structure is observed to be located at multiple-height ledges of the pseudotwin boundary. Fig. 6b shows a lamellar structure composed of four γ variants. Two γ variants γ_D–γ_C on the left-hand side of the figure are in a true twin relationship while, on the right-hand side of the figure, there are three γ variants γ_B–γ_A–γ_B which are also in true twin relationship. Two regions with the 9R struture are formed between variants γ_B and γ_C which have a pseudotwin relationship. Both regions with the 9R structure seem to be located at multiple-height ledges of the pseudotwin boundary. In Fig. 6c, γ_A and γ_B are twin-related variants; the 9R structure is formed at the head of the γ_B lamella. In Fig. 6d, all the lamellae are twin-related γ variants (γ_C or γ_D) and three regions showing a 9R structure are observed to be formed at multiple-height ledges of the twin boundaries.

From the above analysis of Fig. 6 we find the following.

(a) The 9R structure was always formed parallel to the primary twin plane, i.e., it was never observed along a conjugate slip plane. The occurence of the 9R structure parallel to the twin indicates that the primary slip plane is the easiest direction of deformation.

(b) The 9R structure was always formed at the multiple-height ledges of either twin or pseudotwin boundaries. That is the γ variants at both sides of the 9R structure are either twin-related or pseudo-twin-related ordered variants of γ-TiAl. In the crystallography, the multiple-height ledges of a twin or pseudotwin boundary are called an incoherent twin or incoherent pseudotwin boundary.

3.3.2. Crystallographic structure of the 9R

Fig. 7 is the enlargement of the 9R structure in Fig. 6b. The 9R structure may be considered as a close-packed structure with stacking faults on every third close-packed plane in the f.c.c. structure. The stacking sequence is ABC/BCA/CAB/A… . A schematic diagram is shown in Fig. 8.

The selected-area electron diffraction pattern (SADP) taken from the region containing γ_C, γ_D and 9R structure in Fig. 6d is shown in Fig. 9a. Fig. 9b gives the schematic index for Fig. 9a. According to the SADP, the orientation relationship between the 9R structure and the γ-TiAl matrix can be determined as

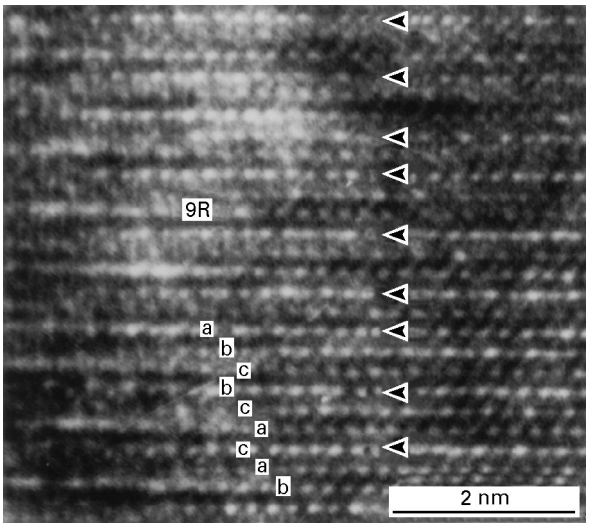

Figure 7 Demonstration of the stacking sequence of the enlarged 9R structure of Fig. 1b; the random stacking faults in 9R structure are also shown (indicated by arrowheads).

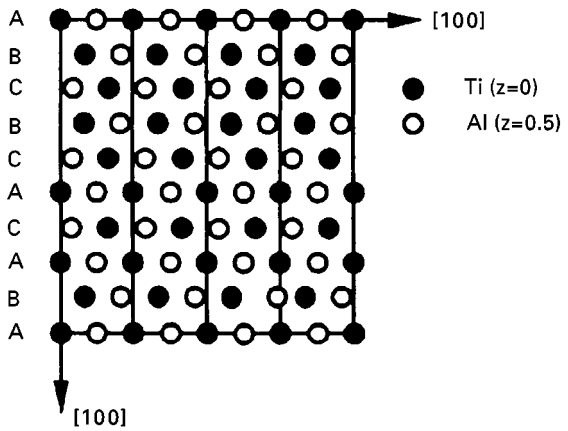

Figure 8 Atomic arrangement of the 9R structure in the [0 1 0] projection. (●) , Ti ($z = 0$) ; (○) , Al ($z = 0.5$).

follows:

$$[0\,1\,0]_{9R}//[1\,0\,\bar{1}]_{\gamma}, (0\,0\,1)_{9R}//(1\,1\,1)_{\gamma}.$$

The 9R structure is an orthorhombic structure. Since the $(0\,0\,1)_{9R}$ planes are the basal planes of the orthorhombic unit cell, it is possible to estimate the lattice parameters for the 9R structure from Figs 8 and 9, based upon the lattice parameter ratio given by Nishiyama and Kajiwara [21] for a perfect 9R structure namely $a:b:c = 1.732:1:7.348$ $(=3^{1/2}:1:3\times 6^{1/2})$. Not accounting for the tetragonality of γ, choosing the lattice parameters to be $a = c = 4.02$Å, and applying the Nishiyama–Kajiwara ratio yield the following unit-cell parameters for the 9R structure:

$$c_{9R} = 9d_{(111)_{\gamma}} = 3^{3/2}a_{\gamma} = 20.8 \text{ Å}$$

$$a_{9R} = d_{(100)_{9R}} = \frac{6^{1/2}}{2}a_{\gamma} = 4.90 \text{ Å}$$

$$b_{9R} = d_{(010)_{9R}} = d_{(101)_{\gamma}} = 2.82 \text{ Å}$$

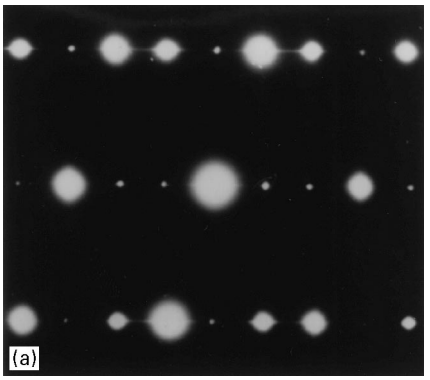

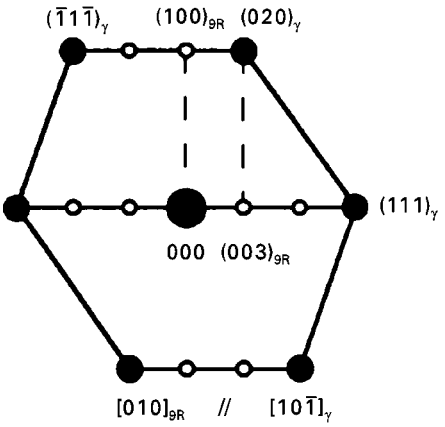

Figure 9 (a) SADP taken along the $[0\,1\,0]_{9R}//[1\,0\,\bar{1}]_{\gamma}$ direction; (b) the schematic index of (a).

4. Discussion

4.1. Mechanism of the stress-induced $\gamma \rightarrow \alpha_2$ phase transformation

The observations in Section 3.1 show that the formation of the DI-α_2 plate is near the misoriented semicoherent α_2–γ_D interface and is an interfacial-related process. As reported in other works [14, 15] and from Fig. 1, there exist many dislocation ledges on the misoriented semicoherent α_2–γ interface and the dislocation characteristic of the ledge is a superdislocation ($\frac{1}{2}[1\,0\,1]$ or $\frac{1}{2}[0\,1\,1]$) or a common dislocation ($\frac{1}{2}[1\,1\,0]$) composed of a $\frac{1}{3}[1\,1\,1]$ Frank partial and a Shockley partial. Under deformation the moving dislocations in γ phase can be absorbed at the α_2–γ interfaces, resulting in the rearrangement of the mismatch interfacial dislocations to accomodate the new interfacial misfit; then density of ledges can be increased and the misoriented semicoherent α_2–γ interfaces can be formed [14, 15]. Furthermore, during thermomechanical deformation process, the dislocations on the misoriented semicoherent α_2–γ interfaces can be emitted from the interface into γ phase by adjusting the deformation of the $\alpha_2 + \gamma$ two-phase alloy. Based on this point, the following dislocation mechanism is proposed for interfacial-related stress-induced $\gamma \rightarrow \alpha_2$ phase transformation.

Under deformation, the interfacial superdislocation $\frac{1}{2}[\bar{1}\,0\,1]$ can move from the interface along $(1\,\bar{1}\,1)$ plane, resulting in the change of γ_D to γ_B. Meanwhile, the interfacial $\frac{1}{3}[1\,1\,1]$ Frank partial dislocation can climb into the γ phase under thermomechanical deformation. Since the $(1\,\bar{1}\,1)$ plane is not a primary slip

plane, after a short distance slip on $(1\,\bar{1}\,1)$ plane the $\frac{1}{2}[\bar{1}\,0\,1]$ superdislocation would move to the $(1\,1\,1)$ primary slip plane through cross-slip and would be dissociated on the $(1\,1\,1)$ plane as follows:

$$\tfrac{1}{2}[\bar{1}\,0\,1] \rightarrow \tfrac{1}{6}[\bar{2}\,1\,1] + \tfrac{1}{6}[\bar{1}\,\bar{1}\,2]$$

The resulting $\frac{1}{6}[\bar{2}\,1\,1]$ Shockley partial dislocation can react with the $\frac{1}{3}[1\,1\,1]$ Frank partial dislocation producing another superdislocation $\frac{1}{2}[0\,1\,1]$. The $\frac{1}{6}[\bar{1}\,\bar{1}\,2]$ Shockley partial dislocation will slip on the primary slip plane $(1\,1\,1)$, resulting in the formation of the stress-induced $\gamma \rightarrow \alpha_2$ phase transformation.

After producing the $\frac{1}{6}[\bar{1}\,\bar{1}\,2]$ Shockley partial dislocations, the first layer of α_2 plate was formed by introducing one Shockley partial on a $(1\,1\,1)$ plane. Subsequent α_2 layers were created by introducing additional Shockley partials of the same type on every other $(1\,1\,1)$ plane.

In fact, the sweep of $\frac{1}{6}[\bar{1}\,\bar{1}\,2]$ Shockley partials on the alternate $(1\,1\,1)$ plane can only induce the structure change from $L1_0$ to a hexagonal close packed (h.c.p.). This h.c.p. structure is not a perfect α_2 phase for its composition is lean for Ti atoms. Thus, during the stress-induced $\gamma \rightarrow \alpha_2$ transformation process, a change to a perfect α_2 phase will need a local short-range diffusion of atoms simultaneously. If, after the generation of the h.c.p. structure, a local short-range diffusion occurs, the h.c.p. plate may gain Ti atoms to change to a perfect α_2 phase, and the composition change results in a change in lattice constants and also interfacial dislocations are introduced to accomodate the misfit in the interface. So, it is probable that the existence of interfacial dislocations can be used to distinguish whether atom transportation occurs. In the present study, when the DI-α_2 plate is small or in its initial stage, the DI-α_2–γ_B and γ_B–α_2 interfaces are nearly free from dislocation ledges (see Fig. 2). When the DI-α_2 plate is well grown, the DI-α_2–γ_B and γ_B–α_2 interfaces have many dislocation ledges (see Fig. 3). This means that, at the initial stage of the stress-induced $\gamma \rightarrow \alpha_2$ transformation, no atom transportation occurs, while the DI-α_2 grows to some stage a local short-range or long-range diffusion of atoms occurs.

4.2. Mechanism of the stress-induced $\alpha_2 \rightarrow \gamma$ phase transformation

From Fig. 4, it can be concluded that the nucleation of the DI-γ plate occurs at the α_2–γ interface, and the growth of the DI-γ plate occurs via the propagation of $\frac{1}{6}\langle 1\,0\,\bar{1}\,0\rangle$ Shockley partials moving on the alternate $(0\,0\,0\,1)_{\alpha_2}$ planes in coordination. In the situation in this study, the DI-γ plate was nucleated at the misoriented semicoherent α_2–γ_D interface. According to the work of Zhao and Tangri [22] and Wunderlich *et al.* [23], at the α_2–γ interface, not only TiAl but also Ti_3Al contain interfacial dislocations which accommodate the lattice misfit between both phases. The interfacial dislocations which are contained in the Ti_3Al phase of a misoriented semicoherent α_2–γ_D interface are mainly $(\frac{a}{6})\langle 1\,1\,\bar{2}\,0\rangle$ partials for the $\frac{1}{3}[1\,1\,1]$ Frank partials are predominantly in the TiAl phase. During deformation, the $(\frac{a}{6})\langle 1\,1\,\bar{2}\,0\rangle$ can be emitted from the interface and undergoes the following dissociation:

$$(\tfrac{a}{6})\langle 1\,1\,\bar{2}\,0\rangle \rightarrow (\tfrac{a}{6})\langle 1\,0\,\bar{1}\,0\rangle + (\mathrm{APB} + \mathrm{SISF}) + (\tfrac{a}{6})\langle 0\,1\,\bar{1}\,0\rangle$$

where APB is an antiphase boundary and SISF is a superlattice intrinsic stacking fault. The reaction occurs on every other α_2 basal plane and, in the present situation, eight reactions occur on the α_2 basal planes resulting in eight $(\frac{a}{6})\langle 1\,0\,\bar{1}\,0\rangle$ Shockley partials on the alternate $(0\,0\,0\,1)_{\alpha_2}$ planes; then they move in coordination into the α_2 phase on the α_2 basal planes, so that the structure change of α_2 to f.c.c. is generated. The stacking sequence of $(0\,0\,0\,1)_{\alpha_2}$ planes ABAB … is altered to that of $(1\,1\,1)_{\mathrm{f.c.c.}}$ planes ABCABC … . The f.c.c. structure must gain Al atoms to adopt the composition of the γ phase. A local short-range diffusion will be needed. Zhang *et al.* [12] claimed that no atomic transportation is involved and that the DI-γ phase is lean in Al. For the shown DI-γ lath, the DI-γ–α_2 interface is free from ledges. This means that few interfacial dislocations are introduced to accommodate the misfit in the interface which mainly results from the tetragonality of the γ phase. So it appears that there is no atom transportation during this stress-induced $\alpha_2 \rightarrow \gamma$ transformation, for the composition change would result in the tetragonality of DI-γ plate (a c/a ratio larger than one) and this would introduce interfacial dislocations in the DI-γ–α_2 interface.

Fig. 5 provides further evidence for a stress-induced $\alpha_2 \rightarrow \gamma$ transformation. The nucleation of the DI-γ plate is from the stacking fault on the basal plane of the α_2 phase. Such a stress-induced feature may be attributed to the movement of the $(\frac{a}{6})\langle 1\,0\,\bar{1}\,0\rangle$ Shockley partials on the alternate $(0\,0\,0\,1)_{\alpha_2}$ planes induced by some particular deformation mechanisms. Since the DI-γ plate is only three or four layers thick, it is conceivable that no long-range atomic transport is needed for such a stress-induced $\alpha_2 \rightarrow$ DI-γ transformation. Further work is being carried out to characterize the process in more detail.

4.3. Formation mechanism of the 9R structure

As indicated in Section 3.3, the 9R structure was always found to have formed at incoherent twin or incoherent pseudotwin boundary. The interfacial dislocation structures of these incoherent twin and incoherent pseudotwin boundaries can account for the formation of the 9R structure.

If we neglect the tetragonality of the $L1_0$ structure of γ-TiAl, we can treat incoherent twin or incoherent pseudotwin boundaries of γ-TiAl as that of a f.c.c. structure. Fig. 10 illustrates the atomic structure of an incoherent twin boundary in the γ-TiAl phase viewed along a $[1\,\bar{1}\,0]_m/[\bar{1}\,1\,0]_T$ direction. Following the analysis procedure of the Read circuit construction for the determination of the Burgers vectors of the grain-boundary dislocations [24], here a Read circuit is constructed so that the closure failure from F_2 to

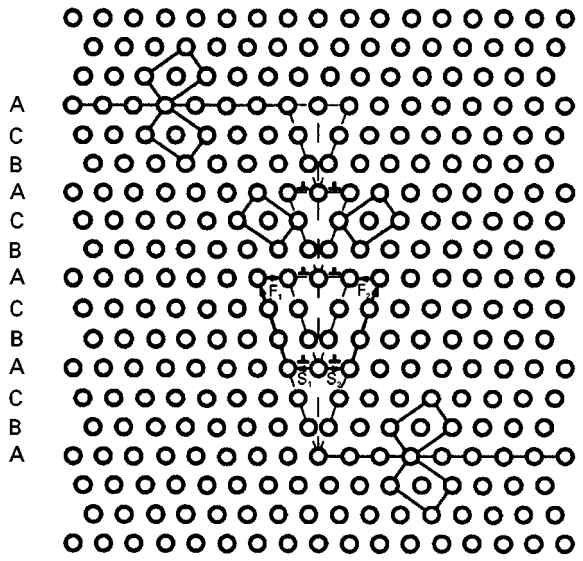

Figure 10 Schematic representation of an incoherent twin boundary. The Read circuit construction for the determination of the Burgers vectors of the grain-boundary dislocations is also shown.

F_1 is defined as the Burgers vector of the grain-boundary dislocation in the "start to finish — right hand" sense. The dislocation arrangement in this grain boundary is identified by the closure failure. In this representation the incoherent twin boundary is seen to be a symmetrical tilt boundary consisting of a stack of edge dislocations with a lattice Burgers vectors. The net Burgers vector of the grain-boundary dislocation, i.e., the vector connecting F_2 and F_1, is $2 \times \frac{1}{6}[1\,1\,\bar{2}]$. One of the two Shockley partial dislocations is in the twin and one belongs to the matrix. During deformation the interfacial Shockley partial dislocation in the matrix may glide on a $(1\,1\,1)_\gamma$ plane into the matrix. As inferred from Fig. 10 the spacing D between the regularly spaced interfacial Shockley partial dislocations is three $(1\,1\,1)_\gamma$ atomic planes and, then, during deformation a Shockley partial is moved on every third $\{1\,1\,1\}_\gamma$ plane, giving rise to the observed stacking sequence (Figs 7 and 8) of the 9R structure. Therefore, the 9R structure can be produced by the glide of these regularly spaced Shockley parital dislocations located on an incoherent twin boundary on every third close-packed plane.

4.4. Random stacking faults in the 9R structure

The 9R structure can be considered to consist of a periodic array of hexagonal stacking on every third close-packed plane in a perfect f.c.c. stacking sequence. Additional stacking faults can occur randomly on close-packed planes in the 9R structure. Such random stacking faults were identified in the HTREM images (Fig. 6) by variations in the regular 9R fringes with the three-layer modulation seen parallel to the basal planes.

According to the analysis of previous studies [25–28], a number of different random stacking faults are possible for the 9R structure. These are shear- and sequence-type faults, which are distinguished by the mechanism for their formation. They can be hexagonal-, cubic- or twin-type faults, which are distinguished by the local stacking structure in the vicinity of the fault. Dark-field TEM investigations [25] and direct imaging using HRTEM [26–28] both revealed cubic- and hexagonal-type sequence faults on the 9R basal planes of Cu-based alloys but failed to find evidence for twin-type sequence faults or any shear-type faults. Cubic or hexagonal faults produce a fringe spacing of four or two layers, respectively, at the position of the fault in HRTEM images.

From the enlarged HRTEM images of the 9R structure in Fig. 7, it is possible to distinguish regions in the 9R fringe patterns where the three-layer spacing is replaced by a two-layer spacing (indicated by arrowheads). This indicates that random stacking faults are present within the 9R structure.

5. Conclusions

Stress-induced $\gamma \rightarrow \alpha_2$, $\alpha_2 \rightarrow \gamma$ and $\gamma \rightarrow 9R$ phase transformations in a hot-worked Ti–45 at% Al–10 at% Nb alloy with nearly fully lamellar microstructure were investigated by HRTEM.

1. The stress-induced $\gamma \rightarrow \alpha_2$ phase transformation is an interface-related process. The interfacial superdislocations emitted from the misoriented semicoherent α_2–γ interface react with each other or with the moving dislocations in the γ phase, resulting in the formation of the stress-induced α_2 phase. Meanwhile, the orientation of the γ phase, with an interface along which the interfacial superdislocation moves, was also changed. The structure of the dislocation ledges plays an important role in the formation of the stress-induced α_2 phase.

2. The observed stress-induced $\alpha_2 \rightarrow \gamma$ phase transformation can either be nucleated at α_2–γ interfaces or at the stacking faults on the basal plane of the α_2 phase. The growth of the DI-γ plate is accomplished by the glide of $(\frac{a}{6})\langle 1\,0\,\bar{1}\,0\rangle$ Shockley partials on the alternate basal plane $(0\,0\,0\,1)_{\alpha_2}$ and the $(\frac{a}{6})\langle 1\,0\,\bar{1}\,0\rangle$ Shockley partials move in coordination rather than on the $(0\,0\,0\,1)_{\alpha_2}$ plane one by one. It appears that there is no atom transportation during the stress-induced $\alpha_2 \rightarrow \gamma$ transformation.

3. The 9R structure was always found to form at incoherent twin or incoherent pseudotwin boundaries. During deformation, interfacial Shockley partial dislocations on these incoherent twin and incoherent pseudotwin boundaries may glide on $(1\,1\,1)_\gamma$ planes into the matrix, resulting in the formation of the 9R structure. Random stacking faults can occur within the 9R structure.

Acknowledgements

The authors would like to thank Professor R. Wagner, GKSS Research Center, Germany, for valuable comments on the manuscript. This project was financially supported by National Nature Science Foundation of China.

References

1. Y. W. KIM, *J. Metals* **46** (1994) 30.
2. Y. W. KIM and D. M. DIMIDUK, *ibid.* **43** (1991) 40.
3. M. A. MORRIS, *Phil. Mag. A* **68** (1993) 237, 259.
4. M. YAMAGUCHI and H. INUI, in: "Structural intermetallics", edited by R. Darolia, J. J. Lewandawski, C. T. Liu, P. L. Martin, D. B. Miracle and M. V. Nathal (The Minerals, Metals and Materials Society, New York, 1993) p. 127.
5. J. G. WANG, PhD thesis, University of Science and Technology Beijing, Beijing (1994).
6. G. L. CHEN, Y. D. HUANG, W. Y. YANG and Z. Q. SUN, in: "Processing, properties and applications of Fe_3Al based aluminides", edited by J. H. Schneibel and M. A. Crimp, Metallurgical Society of AIME, Warendale, PA, (1994) p. 131.
7. S. R. SINGH and J. M. HOWE, *Phil. Mag. Lett.* **65** (1992) 233.
8. F. APPEL, P. A. BEAVEN and R. WAGNER, *Acta Metall. Mater.* **41** (1993) 1721.
9. C. R. FENG, D. J. MICHEL and C. R. CROWE, *Scripta Metall.* **23** (1989) 241.
10. C. R. FENG, D. J. MICHEL and C. R. CROWE, *Mater. Sci. Engng.* **A145** (1991) 257.
11. Y. GAO, J. ZHU, H. SHEN and Y. WANG, *Scripta Metall. Mater.* **28** (1993) 651.
12. Y. G. ZHANG, F. D. TICHEAAR, F. W. SCHAPINK, Q. XU and C. Q. CHEN, *ibid.* **32** (1995) 981.
13. G. L. CHEN, W. J. ZHANG, Y. D. WANG, J. G. WANG and Z. Q. SUN, in "Structural intermetallics", edited by R. Darolia, J. J. Lewandawski, C. T. Liu, P. L. Martin, D. B. Miracle and M. V. Nathal (The Minerals, Metals and Materials Society, New York, 1993) p. 319.
14. G. L. CHEN, J. G. WANG, L. C. ZHANG and H. Q. YE, *Acta Metall. Sin.* (*Engl. Lett.*) **8** (1995) 273.
15. J. G. WANG, L. C. ZHANG, G. L. CHEN and H. Q. YE, unpublished research (1996).
16. J. G. WANG, G. L. CHEN, L. C. ZHANG and H. Q. YE, in Proceedings of Second International Symposium on Structural Intermetallics, Seven Springs, 1997, submitted.
17. J. G. WANG, L. C. ZHANG, G. L. CHEN and H. Q. YE, *Scripta Metall. Mater.* **37** (1997) 135.
18. J. G. WANG, G. L. CHEN, L. C. ZHANG and H. Q. YE, *Mater. Lett.* **31** (1997) 179.
19. Y. S. YANG and S. K. WU, *Scripta Metall. Mater.* **24** (1990) 1801.
20. Y. S. YANG and S. K. WU, *Phil. Mag. A* **65** (1992) 15.
21. Z. NISHIYAMA and S. KAJIWARA, *Jpn. J. Appl. Phys.* **2** (1963) 478.
22. L. R. ZHAO and K. TANGRI, *Phil. Mag. A* **64** (1991) 361.
23. W. WUNDERLICH, T. KREMSER and G. FROMMEYER, *Z. Metallkde* **81** (1990) 802.
24. J. P. HIRTH and R. W. BALLUFFI, *Acta Metall.* **21** (1973) 929.
25. M. ANDRADE, M. CHANDRASEKARAN and L. DELAEY, *ibid.* **32** (1984) 1809.
26. J. M. COOK, M. A. O'KEEFE, D. J. SMITH and M. W. STOBBS, *J. Microsc.* **129** (1983) 295.
27. F. C. LOVEY, *Acta Metall.* **35** (1987) 1103.
28. P. J. OTHEN, M. L. JENKINS and G. D. W. SMITH, *Phil. Mag. A* **70** (1994) 1.

Received 9 June 1997
and accepted 5 February 1998